

# Electrical Facility Effects on Hall Thruster Cathode Coupling: Performance and Plume Properties

Jason D. Frieman,\* Jonathan A. Walker,† and Mitchell L. R. Walker‡  
*Georgia Institute of Technology, Atlanta, Georgia 30332*

Vadim Khayms§  
*Lockheed Martin Space Systems Company, Sunnyvale, California 94089*  
and

David Q. King¶  
*Aerojet Rocketdyne, Inc., Redmond, Washington 98052*

DOI: 10.2514/1.B35683

The impact of facility conductivity on Hall effect thruster cathode coupling is experimentally investigated. The 3.4 kW Aerojet Rocketdyne T-140 Hall effect thruster operating at a discharge voltage of 300 V, a discharge current of 10.3 A, and an anode flow rate of 11.6 mg/s serves as a representative Hall effect thruster test bed. The nominal facility operating pressure during thruster operation is  $7.3 \times 10^{-6}$  Torr corrected for xenon. Two  $0.91 \times 0.91$  m square aluminum plates are placed adjacent to, but electrically isolated from, the walls of the conductive vacuum chamber at two locations with respect to the center of the thruster exit plane: 4.3 m axially downstream along the thruster centerline, and 2.3 m radially outward centered on the exit plane. The plates and body of the Hall effect thruster are configured in three distinct electrical configurations with corresponding measurements: 1) electrically grounded with measurements of currents to ground, 2) electrically isolated with measurements of floating voltages, and 3) isolated from ground but electrically connected with measurements of the current conducted between the plates. Measurements are taken as the radial position of the cathode is varied from 0 to 129 cm with respect to the nominal cathode location. Measurements of the current collected by the plates and thruster body indicate that cathode electrons preferentially travel to the thruster body, Hall effect thruster plume, and radial facility surfaces for cathode locations in the near field, midfield, and far field, respectively. These results indicate that cathode position alters the recombination pathways taken by cathode electrons in the Hall effect thruster circuit.

## Nomenclature

$B$	=	magnetic field strength, G
$e$	=	elementary charge, C
$I$	=	current, A
$m_e$	=	electron mass, kg
$n_e$	=	electron number density, $m^{-3}$
$n_i$	=	ion number density, $m^{-3}$
$P_b$	=	vacuum chamber base pressure, Torr
$P_c$	=	corrected vacuum chamber background pressure, Torr
$P_i$	=	indicated vacuum chamber background pressure, Torr
$V$	=	voltage, V
$V_{cg}$	=	cathode-to-ground voltage, V
$V_{mp}$	=	most probable ion voltage with respect to ground, V
$V_p$	=	plasma potential with respect to ground, V

$V_{pa}$	=	axial plate voltage with respect to ground, V
$V_{pr}$	=	radial plate voltage with respect to ground, V
$\nu$	=	collision frequency, Hz
$\Omega_e$	=	electron Hall parameter

## I. Introduction

THE high specific impulse, thrust efficiency, and thrust density provided by Hall effect thrusters (HETs) make them an appealing choice for use as the primary propulsion system on board a number of commercial and government Earth-orbiting satellite missions. In addition to the mass savings offered by these performance attributes, developments in in-space power and the growing western flight heritage portfolio of HETs have also increasingly made them prime candidates for more ambitious deep space missions [1].

The growth in interest and popularity of these devices has caused a corresponding increase in HET research and testing. Despite the similarities among the devices tested and measurements recorded at each of these facilities, the wide range of facility geometries, sizes, materials, and pumping capacities makes it difficult for researchers to compare datasets without the inclusion of facility-dependent corrections [2]. It is therefore necessary to develop an understanding of how to quantify facility effects on HET operation and data collection so that facility-dependent testing artifacts can be corrected for and a facility-independent understanding of the device performance can be achieved.

Although several investigations into facility effects exist in the literature, most of them focus on the role of facility backpressure on plume properties and device operation. Previous studies have shown that increases in facility pressure result in artificial increases in device thrust and efficiency due to neutral ingestion or entrainment [3–13]. Work has also been conducted linking background pressure to parasitic facility effects caused by resonant charge exchange (CEX) collisions. Specifically, studies have shown that higher facility pressures lead to increased CEX collisions, which, in turn, introduce

Presented as Paper 2014-3711 at the 50th AIAA/ASME/SAE/ASEE Joint Propulsion Conference, Cleveland, OH, 28–30 July 2014; received 3 December 2014; revision received 22 May 2015; accepted for publication 22 June 2015; published online 17 August 2015. Copyright © 2015 by Jason D. Frieman. Published by the American Institute of Aeronautics and Astronautics, Inc., with permission. Copies of this paper may be made for personal or internal use, on condition that the copier pay the \$10.00 per-copy fee to the Copyright Clearance Center, Inc., 222 Rosewood Drive, Danvers, MA 01923; include the code 1533-3876/15 and \$10.00 in correspondence with the CCC.

\*Graduate Research Assistant, Aerospace Engineering, High-Power Electric Propulsion Laboratory; jfrieman3@gatech.edu. Student Member AIAA.

†Graduate Research Assistant, Aerospace Engineering, High-Power Electric Propulsion Laboratory; jwalker30@gatech.edu. Student Member AIAA.

‡Associate Professor, Aerospace Engineering, High-Power Electric Propulsion Laboratory; mitchell.walker@ae.gatech.edu. Associate Fellow AIAA.

§Electric Propulsion Architect; vadim.khayms@lmco.com. Member AIAA.

¶Technical Fellow, Engineering; david.king@rocket.com. Member AIAA.

additional plume components and artificially increase the ion current density measured by Faraday probes in the regions of the HET plume at large angles with respect to the centerline [3,14–16]. Azziz et al. suggested that the relationship between the current density and background pressure is linear for all angular positions in the HET plume [17]. This body of experimental evidence on pressure effects seeks to develop a process by which to calibrate any vacuum facility in terms of pressure [14].

HET test facilities are also almost ubiquitously metallic and, as such, have finite conductivity. Recent work has indicated that chamber conductivity plays a significant role in the HET electrical circuit, and consequently represents a previously unexplored topic of electrical facility effects [18,19]. Specifically, this work has shown that the facility walls collect a significant fraction of the discharge current and, as such, act as an alternate recombination site for plume ions and electrons that have not undergone recombination before reaching the facility walls. The completion of the recombination process at the wall, as well as the collection of a significant electron current by the facility walls, could significantly alter the path of the electrons in the plume. Instead of being forced to travel in the plasma phase to the HET plume for collisional recombination, a portion of the electrons can instead travel within the facility wall, to be conducted to the recombination site. This alternate pathway is an artificial effect introduced by the presence of the vacuum facility and is expected to be absent on orbit. Thus, any process dependent upon the path of the electrons through the plasma (including plasma reactance and resistance) may be significantly different between ground operation and operation on orbit [18–21].

One of the most important processes related to electron motion through the HET plume is cathode coupling as it affects thrust, specific impulse, radiated electromagnetic interference (EMI), and spacecraft–plume interactions [22]. Specifically, studies have shown that increases in HET thrust, efficiency, and cathode coupling voltages, as well as a reduction in plume divergence angles, can be realized by placing the cathode so that it is axially aligned with the thruster axis and is as close to the HET poles as possible [20–27]. These benefits are maximized for a cathode mounted internally near the HET centerline [24,25]. Varying the radial and axial separation of the cathode from the HET away from this inner position has been shown to decrease the efficiency and increase the magnitude of the cathode coupling voltage [20,21,26,27]. Current explanations for these observed relationships between cathode position and cathode coupling voltage relate these trends to the change in plasma impedance realized when moving the cathode orifice through the magnetic field and, specifically, across field separatrix surfaces [20,21]. However, such theories do not fully account for the losses in coupling efficiency observed with increasing cathode separation distance and cannot explain these phenomena in thrusters that do not exhibit off-centerline separatrices [20,21,26]. Furthermore, they were formulated without any knowledge of the impact of the conductive facility walls on the electron path within a test facility.

This work experimentally investigates the role of a conductive facility on cathode coupling in a HET discharge. A representative facility testbed with a controllable wall bias is created by placing two large square aluminum plates adjacent to, but electrically isolated from, the walls of the vacuum test facility both axially downstream and radially outward from the exit plane of the Aerojet Rocketdyne T-140 HET. To assess the impact of chamber conductivity on cathode coupling, measurements of the current conducted through the plates (as well as the voltage to which the plates are biased) are taken as the plates are electrically isolated, connected, and grounded and as the cathode is moved from a radial separation distance of 0 to 128.8 cm with respect to the nominal location for the T-140 HET. These measurements are taken for both floating and grounded thruster body configurations so that the impact of this surface on electron motion can be determined. To determine the effect of chamber conductance on the plasma plume as well as compare the plume properties to measurements from previous work on radial cathode positioning, measurements of the plasma potential and most probable ion energy are also taken 1 m downstream along the thruster centerline at each cathode position and plate bias.

## II. Experimental Setup

### A. Vacuum Facility

All experiments were performed in Vacuum Test Facility 2 (VTF-2) at the Georgia Institute of Technology High-Power Electric Propulsion Laboratory (HPEPL). A schematic of this facility is shown in Fig. 1. VTF-2 is a stainless-steel chamber measuring 9.2 m in length and 4.9 m in diameter. VTF-2 is evacuated to rough vacuum using one 495 ft<sup>3</sup>/min rotary-vane pump and one 3800 ft<sup>3</sup>/min blower. High vacuum is achieved using 10 CVI TMI reentrant cryopumps. The cryopump shrouds are fed using the Stirling Cryogenics SPC-8 RL special closed-loop nitrogen liquefaction system, detailed by Kieckhafer and Walker [28]. The facility has a combined nominal pumping speed of 350,000 l/s on xenon and can achieve a base pressure of  $1.9 \times 10^{-9}$  Torr. Pressure in VTF-2 was monitored using two Agilent Bayard-Alpert 571 hot-filament ionization gauges controlled by an Agilent XGS-600 gauge controller. One gauge was mounted to a flange on the exterior of the chamber, whereas the other was mounted 0.6 m radially outward centered on the exit plane. To prevent plume ions from having a direct line of sight to the ionization gauge filament of the interior ion gauge and potentially affecting the pressure measurement, a neutralizer identical to the one used by Walker and Gallimore was attached to the gauge orifice [29]. The nominal operating pressure for this work as measured by the interior and exterior ion gauges was  $1.3 \times 10^{-5}$  Torr and  $7.3 \times 10^{-6}$  Torr corrected for xenon, respectively. The corrected pressure,  $P_c$ , was found by relating the indicated pressure,  $P_i$ , and the vacuum chamber base pressure,  $P_b$ , to a gas-specific constant using the following equation [30]:

$$P_c = \left[ \frac{P_i - P_b}{2.87} \right] + P_b \quad (1)$$

### B. T-140 HET

All experiments detailed in this work were performed using the Aerojet Rocketdyne T-140 HET originally developed by Space Power, Inc., in collaboration with the Keldysh Research Center and Matra Marconi Space [31]. The T-140 HET is a laboratory-model HET that has a discharge channel made of M26-grade boron nitride with an outer diameter of 143 mm. The performance of the T-140 has been extensively mapped by prior investigations [31]. The thruster body was isolated from the facility ground, and thus could be electrically configured as either floating or grounded.

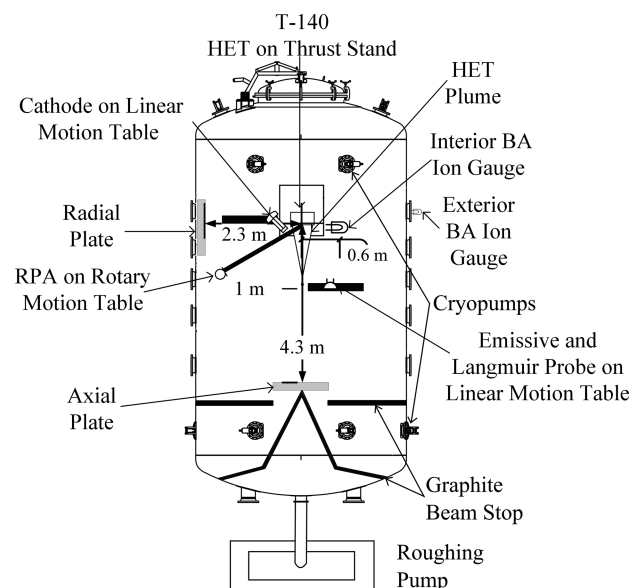


Fig. 1 Schematic of VTF-2 (not to scale). (BA, Bayard-Alpert)

High-purity (99.9995%) xenon propellant was supplied to the thruster and cathode using stainless-steel lines metered with MKS 1179A mass flow controllers. The controllers were calibrated before each test by measuring gas pressure and temperature as a function of time in a known control volume. The mass flow controllers had an uncertainty of  $\pm 0.03$  mg/s (5.1%) for the cathode flow and  $\pm 0.12$  mg/s (2%) for the anode flow [32].

An Electric Propulsion Laboratory (EPL) hollow cathode plasma electron emitter (HCPEE) 500-series cathode was located at the nine o'clock position of the thruster. The cathode flow rate was set to a constant 1.16 mg/s for all thruster operating conditions. The orifice of the cathode was located approximately 2.5 cm downstream of the thruster exit plane at a fixed declination of 55 deg with respect to the thruster centerline. The nominal radial position of the cathode was 18.1 cm outward from thruster centerline. The radial location of the cathode orifice was varied from 0 to 128.8 cm outward from the nominal position using a Parker Daedal 406XR precision linear motion stage with a 2000 mm travel. The positional uncertainty of the motion stage was  $\pm 159$   $\mu$ m. The approximate magnetic field strengths at the cathode orifice as a function of radial location away from the nominal position are shown in Table 1.

The magnetic circuit configuration of the T-140 HET (two concentric coils centered on the thruster centerline) restricts the position of the magnetic field separatrix to the thruster centerline and precludes the T-140 HET from exhibiting the off-centerline separatrix surfaces shown in HETs with magnetic coils centered off axis [18–21,33]. This magnetic field topology eliminates any concerns about the changing nature of the near-field plume properties and cathode coupling as a function of cathode position relative to the absent off-centerline separatrix surface [20].

The T-140 HET discharge was controlled using a Magna-Power TSA800-54 power supply. All other thruster components were powered using TDK-Lambda GEN60-25 power supplies. A TDK-Lambda GEN150-10 and GEN40-38 were used for the cathode keeper and heater, respectively. All electrical connections entered VTF-2 through separate feedthroughs to eliminate potential EMI concerns. The thruster discharge supply was connected to a discharge filter consisting of a 95  $\mu$ F capacitor and 1.3 resistor in order to prevent oscillations over 1.4 kHz in the discharge current from reaching the discharge supply. The circuit used for the T-140 HET in this work is shown in Fig. 2.

The discharge current oscillations of the T-140 HET were recorded using a Teledyne LeCroy CP150 current probe connected to a Teledyne LeCroy HDO6104 oscilloscope. The uncertainty and bandwidth of the current probe were  $\pm 1\%$  and 10 MHz; for the oscilloscope, they were  $\pm 0.5\%$  full scale and 1 GHz. In the floating thruster body configuration, the thruster body floating voltage was measured differentially using Teledyne LeCroy PP018 passive probes with a bandwidth of 500 MHz and accuracy of  $\pm 0.5\%$  connected to the Teledyne LeCroy oscilloscope. When the thruster body was grounded, the current conducted through the thruster body

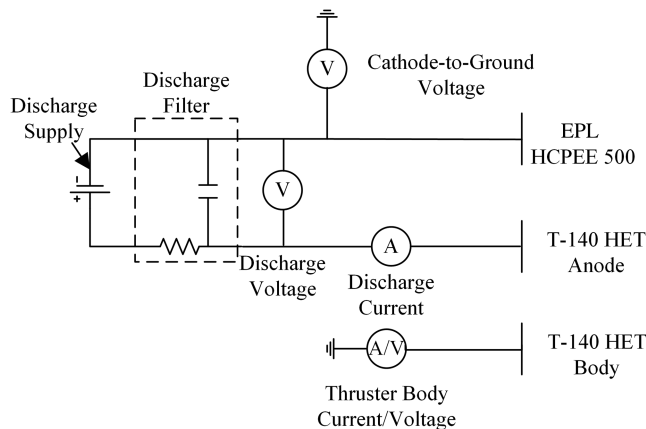


Fig. 2 T-140 HET circuit and thruster telemetry measurement locations.

Table 1 Approximate magnetic field strength as a function of cathode orifice radial location away from nominal position

Radial location, cm	Magnetic field strength, G
0	30
1.3	20
2.5	20
3.8	10
6.4	0

to ground was measured using a Teledyne LeCroy CP030 current probe connected to the Teledyne LeCroy oscilloscope. The CP030 had a bandwidth of 50 MHz and an accuracy of  $\pm 1\%$ .

The mean discharge voltage of the T-140 HET was measured differentially using a pair of Teledyne LeCroy PPE 2 kV 100:1 high-voltage probes connected to a Tektronix TDS3034B oscilloscope. The bandwidth of the voltage probes was 400 MHz; the oscilloscope had an uncertainty and bandwidth of  $\pm 2\%$  and 300 MHz, respectively. The cathode-to-ground voltage was measured differentially using two Tektronix P6139A passive probes connected to the Tektronix oscilloscope, which have a bandwidth of 500 MHz and an accuracy of  $\pm 0.5\%$ . Figure 2 shows the location of each telemetry measurement in the T-140 HET circuit.

All data were collected with the T-140 HET operating at a discharge voltage of 300 V, a discharge power of 3.1 kW, an anode xenon flow rate of 11.6 mg/s, and a cathode xenon flow rate of 1.61 mg/s. The thruster voltage, inner and outer magnet currents, anode mass flow rate, and cathode mass flow rate were held constant for all test configurations. The thruster was run through a 3 h conditioning cycle before data collection in order to allow the thruster and thrust stand to approach thermal equilibrium [34].

C. Configuration of Plates

To simulate a metallic facility with controllable wall bias, two 0.91 m  $\times$  0.91 m  $\times$  0.16-cm-thick square aluminum plates were mounted adjacent to, but electrically isolated from, the walls of the vacuum test facility. The axial plate was located 4.3 m downstream from the exit plane of the thruster. The radial plate was located 2.3 m radially outward from the thruster centerline and was centered on the exit plane of the T-140 HET. Figure 1 shows the physical location of the plates with respect to the T-140 HET. Identical plates have been used in previous studies of electrical facility effects [18,19,33]. The surface area of the plates represents 2% of the total facility wall area.

Figure 3 shows each of the three plate electrical configurations used in this test. In all three cases, the electrical connections to the plates were made using a RG-58 coaxial cable with a grounded shield

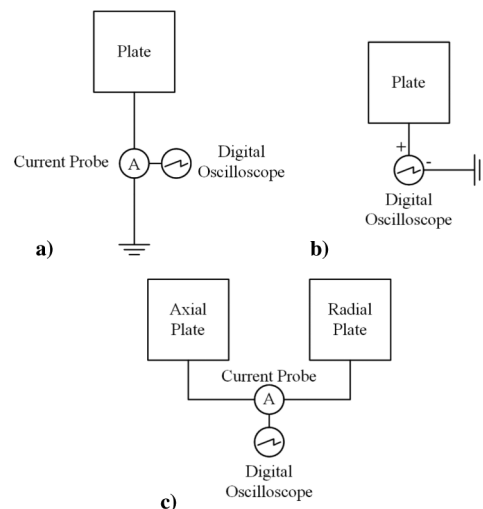


Fig. 3 Plate circuit configurations: a) grounded, b) floating, and c) connected.

that passed through a Bayonet Neill-Concelman feedthrough into the chamber. This transmission line was similar to those previously used to study discharge oscillations in HETs [35,36].

In configuration A (grounded), each plate was directly connected to chamber ground with the current conducted between each plate and ground measured with a Teledyne LeCroy CP030 current probe connected to the Teledyne LeCroy HDO6104 oscilloscope; the plate currents and thruster telemetry signals were measured simultaneously at a sampling frequency of 125 MS/s for 20 ms to eliminate any potential phasing effects that could result from asynchronous sampling. In configuration B (floating), the plates were electrically isolated, and the floating voltage was measured directly using a Teledyne LeCroy PP018 passive probe connected to the Teledyne LeCroy oscilloscope; these voltage measurements were also taken simultaneously with measurements of the T-140 HET discharge current and voltage oscillations at a sampling frequency of 125 MS/s for 20 ms. In configurations A and B, both plates were simultaneously grounded or floated, respectively. In configuration C (connected), the plates were connected to each other instead of to ground, and the current conducted between the two plates was measured with a Teledyne LeCroy CP030 current probe connected to the Teledyne LeCroy oscilloscope; the current conducted between the two plates and the discharge current were measured simultaneously at a sampling frequency of 125 MS/s for 20 ms.

#### D. Thrust Stand

Thrust was measured using the null-type inverted pendulum thrust stand of the NASA John H. Glenn Research Center design detailed in the work of Xu and Walker [37]. The thrust stand consisted of a pair of parallel plates connected by a series of four flexures that supported the top plate and permitted it to deflect in response to an applied force. The position of the upper plate was measured using a linear variable differential transformer (LVDT) and was controlled using two electromagnetic actuators. During operation, the current through each actuator was controlled using a pair of proportional-integral-derivative control loops that used the LVDT signal as the input and then modulated the current through the actuators in order to remove any vibrational noise (damper coil) and hold the upper plate stationary (null coil). The thrust was correlated to the resulting current through the null coil that was required to keep the upper plate stationary. To maintain thermal equilibrium during thruster firings, the thrust stand was actively cooled using three parallel loops: one each through the structure, the null coil, and the outer radiation shroud. Cooling water was supplied by a 1100 W VWR International 1173-P refrigerated recirculation chiller and did not vary by more than 5°C as compared to the thruster-off condition [37].

The thrust stand is calibrated by loading and offloading a set of known weights that span the full range of expected thrust values. A linear fit is then created in order to correlate null coil current to force applied to the thrust stand. To minimize the thermal drift of the zero position, the T-140 HET is initially fired for 3 h at the 3.1 kW nominal operating point to permit initial heating of the system to near thermal equilibrium before the first calibration and is then shut down every 40–60 min so that a recalibration can be performed. The thrust stand uncertainty for this work is  $\pm 3$  mN ( $\pm 1.7\%$  full scale).

#### E. Retarding Potential Analyzer

The ion voltage distribution in the thruster plume was measured using a retarding potential analyzer (RPA). The RPA uses a set of electrostatically biased grids to act as a high-pass voltage filter and selectively filters ions based on the ion voltage [38,39]. The RPA was positioned on an arc located  $1 \pm 0.03$  m downstream of the exit plane of the T-140 HET. The location of the RPA along the arc was controlled using a Parker Daedal 200RT-series rotary table, which had an accuracy of 0.17 deg. All measurements for this work were taken along the thruster centerline.

The four-grid RPA design similar to the one previously used by Xu was used for this work [40]. The grids are (in order from the plasma to the collector) the floating grid, the electron repelling grid, the ion retarding grid, and the electron suppression grid. The floating grid

minimizes plasma perturbations caused by the presence of the probe. The electron repelling grid is biased to  $-30$  V relative to facility ground in order to prevent plasma electrons from reaching the collector. The electron suppression grid is also biased to  $-30$  V relative to facility ground in order to repel any secondary electrons emitted by the collector and promote the recollection of these secondary electrons by the collector in order to remove the effects of secondary electron emission from the current-voltage (I-V) characteristic. The ion retarding grid is biased positive relative to the ground in order to impede the motion of the incident ions, and thus filter the ion population based upon directed kinetic energy per unit charge. Each grid is made of 316 stainless steel, and has a 2.29 cm collection diameter and 31% transparency.

In this work, the electron suppression and repelling grids were both biased to  $-30$  V using two TDK-Lambda GENH 60-12.5 power supplies. The ion repulsion grid bias was controlled by a Keithley 2410 1100 V SourceMeter, and the collector current was measured using a Keithley 6487 picoammeter. The SourceMeter and picoammeter were simultaneously controlled using a LabView virtual instrument to ensure synchronous recording of the ion retarding voltage and collector current.

During each measurement, the ion retarding voltage was swept between ground and 450 V above ground in 2 V increments with a 300 ms dwell time. Two sweeps of the ion retarding voltage were taken at each measurement condition. The resulting I-V traces from each of these sweeps were differentiated with respect to voltage using Newton's difference quotient. The derivative curves were smoothed using the locally weighted scatter plot smoothing algorithm (LOESS) to remove noise. The resultant derivative peak location corresponds to the most probable ion voltages. These voltages are first corrected by subtracting the plasma potential from the most probable values and then averaged together in order to obtain an average most probable ion voltage for each combination of cathode position, plate configuration, and thruster body configuration. This method results in an error of approximately  $\pm 10$  V for the most probable voltage [40,41].

#### F. Emissive Probe

The plasma potential in the thruster plume was measured using an emissive probe. The axis of the probe was oriented parallel to the T-140 HET centerline axis, and the probe tip was located 1 m downstream of the exit plane of the T-140 HET. The position of the emissive probe was controlled using a Parker Daedal 406XR precision linear motion stage; the motion stage had a 2000 mm travel and a positional uncertainty of  $\pm 159$   $\mu$ m. All measurements were taken along the T-140 HET centerline. The probe tip used for this work was constructed from a 0.13-mm-diam loop of thoriated tungsten wire housed in a 4.8-mm-diam double-bore alumina tube.

In this work, the heating current was controlled using a Xantrex XPD 60-9 power supply. A Keithley 2410 1100 V SourceMeter was used to synchronously control the probe bias and measure the probe current.

The inflection point method was used for data collection and analysis. In this method, the probe was heated and then the probe current was monitored as the probe bias was swept in a manner similar to that used with Langmuir probes. The changing characteristic of the probe current trace as a function of applied bias voltage was then used to determine the plasma potential [42]. During each measurement, the heating current to the emissive probe filament was varied over five heating current values. These heating current values varied throughout the probe lifetime, but they were within a range between 1.2 and 1.8 A. One bias sweep was taken per heating current. During each bias sweep, the probe voltage was varied over a range of 0 to 50 V in 1 V increments, with a 300 ms dwell time. The inflection point was then found in each of the I-V traces for each of the different heating current levels, and the plasma potential was found by linearly extrapolating these values to zero emission [42]. The derivative curves used to determine the inflection point were smoothed using a LOESS algorithm to remove noise. The uncertainty associated with this method was approximately  $\pm 0.5$  V [42].

### G. Langmuir Probe

The ion and electron number densities were measured using a cylindrical Langmuir probe. The probe used in this work was constructed using a 0.13-mm-diam 18.3-mm-long tungsten tip housed inside an alumina tube. The tip was bent into a right angle such that the normal to the collecting surface was oriented parallel to the device centerline axis. The transverse orientation of the collecting surface relative to the ion flow direction was chosen in order to avoid the increased ion collection due to collisional and end effects observed for Langmuir probes oriented parallel to the direction of bulk motion in supersonic flowing plasmas [43]. The position of the Langmuir probe was controlled using the same Parker Daedal 406XR precision linear motion stage used to control the emissive probe position. The Langmuir and emissive probes were mounted  $16.5 \pm 0.2$  cm apart on the linear motion stage in order to ensure that no sheath interaction occurred between the two probes. All measurements were taken along the T-140 HET centerline, 1 m downstream of the thruster exit plane. Because all RPA, emissive probe, and Langmuir probe measurements were taken at this location, the linear and rotary motion stages were used to remove each probe from the plume when measurements were not being taken and permit the other probes to be placed at the measurement location.

A Keithley 2410 1100 V SourceMeter was used to synchronously control the probe tip bias and measure the collected current. During each current-voltage sweep, the tip voltage was varied over a range of  $-50$  to  $50$  V in  $0.2$  V increments, with a  $300$  ms dwell time. Two sweeps were taken per measurement and averaged together before processing. The results were interpreted using the orbital-motion-limited theory [44,45]. The uncertainties in ion and electron density measurements with this method were  $\pm 40\%$  [44,46].

## III. Results and Discussion

### A. Plate and Thruster Body Measurements

#### 1. Configuration A: Grounded Plates

Previous work has shown that the primary electrical facility effect on the HET circuit is the establishment of alternative recombination pathways for the ions and electrons in the HET plume [18,19]. Therefore, in order to understand the impact of electrical facility effects on HET cathode coupling, the sensitivity of these pathways to cathode position must first be analyzed. Once presented, the subsequent effects of these pathway sensitivities on the HET circuit can be determined using the measurements shown in Fig. 2. Finally, the resultant changes in HET circuit voltages and plume properties can be analyzed and used to determine the link between electrical facility effects on cathode coupling and HET performance.

Figures 4a and 4b show the time-averaged discharge current and the current collected by the axial and radial plates as a function of cathode position in the grounded-plate configuration shown in Fig. 2b; data are shown for both the grounded and floating thruster body configurations. Net ion current collection is indicated as positive current, and net electron current collection is indicated as negative current. Overall, the axial plate collects a net ion current and the radial plate collects a net electron current for all cathode positions. In the grounded-body configuration, the current collected by the axial and radial plates shows three distinct regions of behavior with respect to cathode distance from the nominal location. For cathode displacements less than and equal to  $2.5$  cm away from the nominal location (indicated as region 1 in both Figs. 4a and 4b), the currents collected by the axial and radial plates have a nonmonotonic dependence on cathode displacement. Specifically, the magnitude of the currents collected by both the axial and radial plates initially decreases in magnitude by  $30$  and  $20\%$ , respectively, and then it increases in magnitude by  $15$  and  $40\%$ , respectively. Nevertheless, the ion current collection by the axial plate still shows an overall decreasing trend with increasing cathode displacement within this region.

For cathode displacements between  $2.5$  and  $29.2$  cm away from the nominal location (indicated as region 2 in both Figs. 4a and 4b), the magnitude of the net ion current collected by the axial plate and the net electron current collected by the radial plate both decrease by approximately  $40\%$ . The discharge current in this region remains nearly constant and has a maximum deviation of approximately  $3\%$ . For cathode displacements greater than  $29.2$  cm away from the nominal location (indicated as region 3 in Fig. 4a), the magnitudes of both the ion current collected by the axial plate and the electron current collected by the radial plate increase with increasing cathode displacement. The axial plate collected current increases by  $27\%$ , and the radial plate collected current increases by  $431\%$ . The discharge current in this region also remains largely invariant and has a maximum deviation of approximately  $3\%$ .

The current collected by the plates as a function of increasing cathode displacement for the floating-body configuration follows the same regional trends observed for the grounded-body configuration. The variations between the plate currents measured for the floating and grounded thruster bodies are  $6$  and  $-11\%$  for the axial and radial plates, respectively. Therefore, in the floating thruster body configuration, the axial plate collects slightly more ion current, whereas the radial plate collects slightly less electron current. The average variation in the discharge current between the floating and grounded thruster body configurations is also small; the average percent difference in discharge current between the floating- and grounded-body configurations is approximately  $2\%$ .

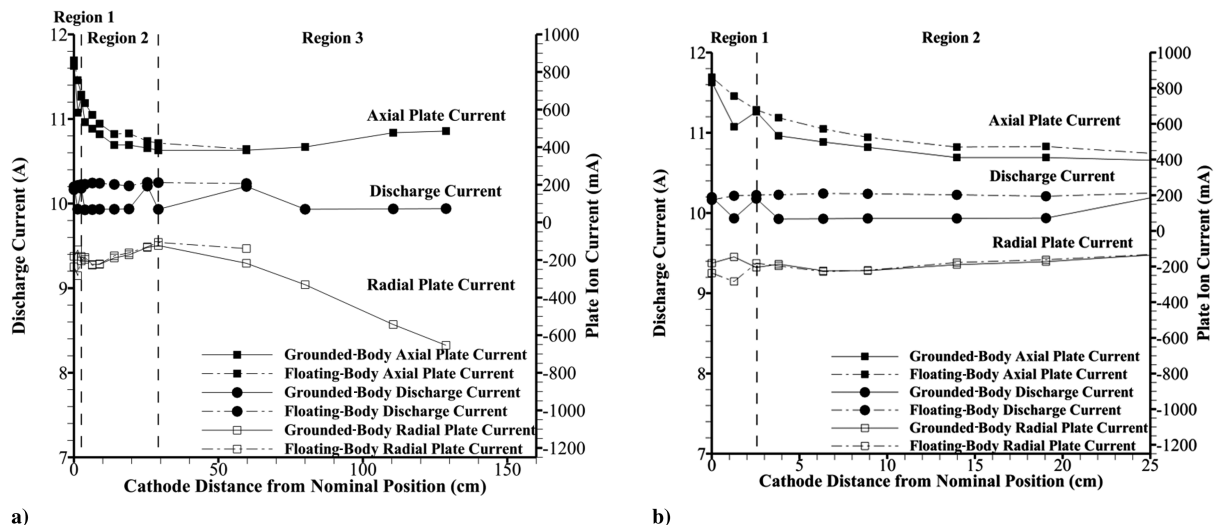


Fig. 4 Discharge current and grounded-plate currents as a function of cathode position: a) all cathode displacements, and b) near-field cathode displacements. Experimental error is within the symbol borders.

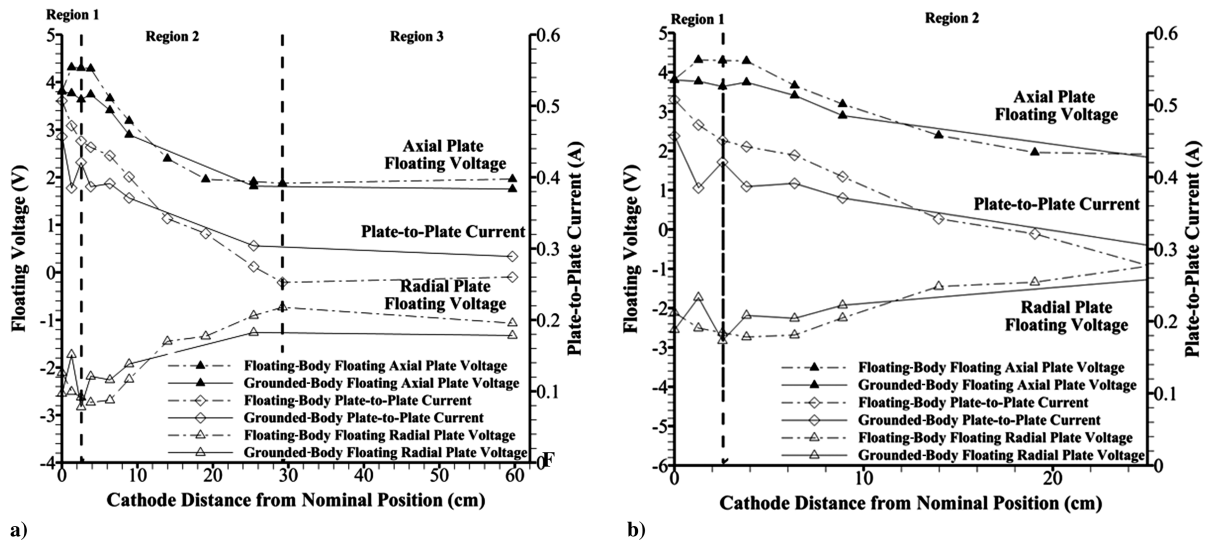


Fig. 5 Plate floating voltages as a function of cathode position: a) all cathode displacements, and b) near-field cathode displacements. Experimental error is within the symbol borders.

## 2. Configurations B and C: Floating and Connected Plates

Figures 5a and 5b show the time-averaged floating voltages and current conducted from the axial plate to the radial plate as a function of cathode position for the floating and connected-plate configurations shown in Figs. 2b and 2c, respectively; data are shown for both the grounded- and floating-body configurations. In the grounded-body configuration, the plate floating voltages also show three distinct regions of behavior with respect to cathode position. The boundaries of these regions are identical to those described previously for the grounded plates. In region 1, the floating voltage of the axial plate decreases monotonically with increasing cathode distance by a total of 4% over the entire region. The floating voltage of the radial plate, however, behaves nonmonotonically; it first decreases in magnitude by 32%, and then it increases back to within 11% of the floating voltage measured at the nominal cathode location. In region 2, the floating voltage magnitude of both the axial and radial plates decreases with increasing cathode displacement. Over this region, the axial plate floating voltage decreases by approximately 50% and the radial plate floating voltage decreases in magnitude by approximately 55%. In region 3, the floating voltages of the axial and radial plates are largely invariant with cathode position; the axial plate floating voltage decreases by 3%, and the radial plate floating voltage decreases by approximately 5%. These trends also hold for the floating-body configuration, which has an average percent difference with respect to the grounded-body configuration of  $-3$  and  $6\%$  for the axial and radial plates, respectively.

The plate-to-plate current measurements shown in Figs. 5a and 5b for the grounded-body configuration also show three regions of behavior with identical demarcations to those present for the floating and grounded plates. In region 1, the current conducted from the axial plate to the radial plate initially maximizes and then decreases by approximately 16% before increasing to within 8% of the value measured at the nominal cathode location. In region 2, the plate-to-plate current decreases with cathode displacement and decreases by a total of 38% over the entire region. In region 3, the current conducted between the plates increases by 5% within the region. These trends are also present for the floating-body configuration. As compared to the grounded-body configuration, the floating-body plate-to-plate current is larger in magnitude by an average of 12% within region 1 and half of region 2, and it is smaller in magnitude in the remainder of region 2 and all of region 3 by an average of 10%.

## 3. Thruster Body

Figure 6 shows the time-averaged discharge current, the current collected by the T-140 HET thruster body in the grounded configuration, and the floating voltage of the T-140 HET thruster

body in floating-body configuration as a function of cathode position and plate electrical configuration. The discharge current shown in Fig. 6 is the average taken across all plate and thruster body configurations. To facilitate comparisons, the lines demarcating the regions previously defined for the grounded, floating, and connected-plate configurations are also included in Fig. 6. Overall, the grounded thruster body collects a net electron current for all plate configurations and cathode locations. The magnitude of this current ranges between 1 and 13% of the discharge current. In the floating configuration, the thruster body has a negative floating voltage with respect to ground that varies between  $-28$  and  $-17$  V. The discharge current of the T-140 HET changes by less than 3% for all cathode locations, and therefore remains largely constant as the cathode displacement and thruster body configuration are changed.

Consistent with the results for the grounded, floating, and connected plates, the current conducted through the grounded thruster body also shows three regions of behavior with respect to cathode position. In region 1, the electron current collected by the thruster body decreases with increasing cathode displacement. Within the region, the total decrease in collected current is 0.4 A. In region 2, the magnitude of the electron current collected by the body continues to decrease with increasing cathode displacement, but at a

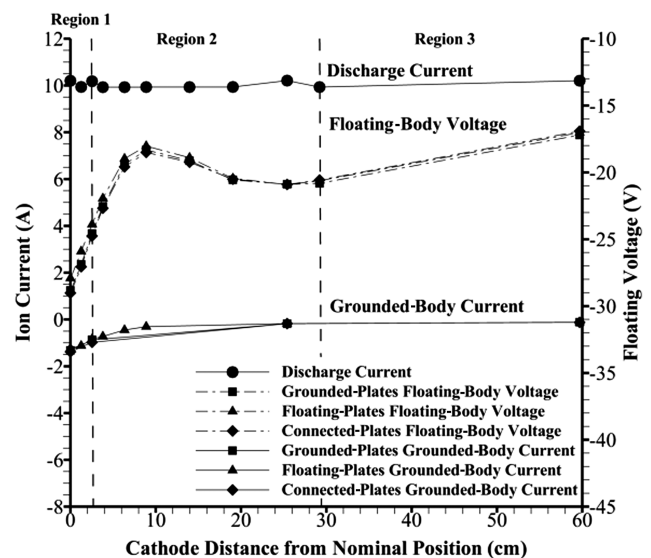


Fig. 6 Discharge current, grounded-thruster-body current, and floating voltage of the thruster body at each cathode position and plate electrical configuration. Experimental error within the symbol borders.

reduced rate; the total decrease within this region is 0.5 A. In region 3, the collected current is almost constant with respect to cathode location, and it decreases by less than 0.1 A between the measurement taken at boundary with region 2 and the one taken at the maximum cathode displacement. These trends are true for every plate electrical configuration, as the current collected by the thruster body is approximately constant between each of the plate electrical configurations.

The variation in thruster body floating voltage with cathode location also follows a regional pattern. In region 1, the floating voltage magnitude decreases with increasing cathode displacement. Specifically, the floating voltage magnitude decreases by a total of 15% between the measurement taken at the nominal location and the measurement taken at a cathode distance of 2.5 cm away from nominal. In region 2, the floating voltage initially continues to decrease in magnitude with increasing cathode displacement by a total of 19%. This trend continues until a cathode distance of 8.9 cm away from nominal. Between cathode distances of 8.9 and 25.4 cm away from nominal, the magnitude of the measured floating thruster body voltage increases by 9%. In region 3, the measured floating voltage again decreases in magnitude by a total of 17%. As with the grounded thruster body configuration, these trends are invariant of the plate electrical configuration.

## B. Plasma Potential Measurements

Previous work has identified that the primary coupling between the conducting walls of the vacuum test facility and the HET circuit is via the plasma potential [18,19]. Therefore, in order to understand the observed trends for the plate and thruster body measurements, the corresponding changes in plasma potential must be analyzed.

Figure 7 shows the plasma-to-ground potential ( $V_p$ , hereafter referred to as the plasma potential) as a function of cathode displacement from the nominal position for each of the plate and thruster body electrical configurations. As shown in Fig. 7, the changes in measured plasma potential with respect to cathode position within region 1 are small (within 8%) for each given plate and thruster body electrical configuration. For cathode locations within region 2, the plasma potential initially sharply increases by an average of 9% as compared to the value measured at the boundary of region 1 and then reaches a near-constant asymptote and changes by less than 1% over the rest of the region. This trend persists into region 3; however, limited data are available within region 3 as potential measurements, for these cathode locations were outside the scope of this experiment. It is important to note that the plasma potential measurements for the grounded-body configuration are all 6% higher on average than those measured for the floating-body configuration.

## C. Discussion of Regional Behavior

### 1. Region 1

As mentioned previously, the current collected by the grounded plates, the floating voltage measured by the radial plate, and the plate-to-plate current conducted between the connected plates shows nonmonotonic behavior in region 1. Specifically, the magnitude of the current collected by the grounded axial and radial plates first decreases significantly, and then increases as the cathode is moved outward in region 1. These changes in magnitude are identical in form to the changes in average discharge current also present in this region. As shown in previous works, the current collection by the grounded plates is driven by the discharge current [18,19]. Therefore, these nonmonotonic fluctuations in magnitude are due to changes in the discharge current observed between cathode locations within this region.

This corresponding change in discharge current also explains the observed decrease in the magnitude of the radial plate floating voltage for the second cathode position. The decrease in discharge current results in fewer electrons being emitted by the cathode, and thus fewer electrons impinging upon the radial plate. This means that the plate has to float less negative in order to repel the required electron flux to maintain the floating boundary condition. It has previously been shown that the plate-to-plate current is driven by the

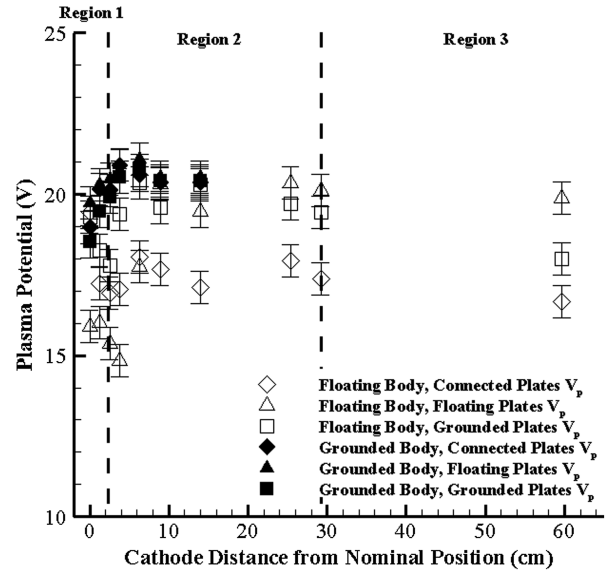


Fig. 7 Plasma potential as a function of cathode location for all thruster body and plate electrical configurations.

difference in floating potential between the axial and radial plates [18,19]. Therefore, the decreased plate-to-plate current is due to the reduced potential difference between the plates driven by the decrease in the magnitude of the radial plate floating voltage.

As shown in Figs. 4a and 4b, within region 1, the percentage of the discharge current collected as electron current by the grounded radial plate is largely constant with respect to cathode position for both thruster body electrical configurations. This invariance, neglecting the aforementioned changes due to the observed changes in discharge current, is also shown by the plate floating voltages and plate-to-plate currents in Fig. 5a. However, the current collected by the thruster body and the axial plate, as well as the magnitude of the thruster body voltage, decreases with cathode displacement in this region, as shown in Fig. 6. The current collected by the axial plate reaches its maximum value within this region. In the floating- and connected-plate configurations, the magnitude of the floating voltage of the axial and radial plates as well as the current conducted between the plates also reach their maximum within this region, as does the electron current collected by the grounded thruster body. However, the floating voltage of the floating thruster body is a minimum for cathode positions within region 1. Lastly, as shown in Fig. 7, the plasma potential increases to near its maximum value with increasing cathode displacement within this region.

These trends are all explained by the strong magnetic field relative to the temperature of the electrons present at the cathode orifice for cathode positions within region 1. The impact of the magnetic field on the motion of the cathode electrons can be described using the electron Hall parameter  $\Omega_e$ , which is defined as a function of the elementary charge  $e$ , magnetic field strength  $B$ , electron mass  $m_e$ , and the total collision frequency  $\nu$  in Eq. (2) [6,47]:

$$\Omega_e = \frac{eB}{m_e \nu} \quad (2)$$

The electron Hall parameter is a measure of the number of gyroradii completed around a magnetic field line by an electron per collision with a neutral atom or ion [6,47]. As the cross-field motion of the electron is enabled by these collisions, the higher the electron Hall parameter, the fewer the collisions that an electron undergoes per gyroradius, and thus the more the motion of the electron gyrocenter follows the magnetic field line [48]. Using the known values of magnetic field strength shown in Table 1 and the cathode electron collision frequencies calculated by Goebel and Katz [6] and Katz et al. [49] for an estimated cathode electron temperature of 6 eV and exit plane neutral density of  $1 \times 10^{18} \text{ m}^{-3}$ , Eq. (2) can be used to evaluate the approximate Hall parameter for each cathode location

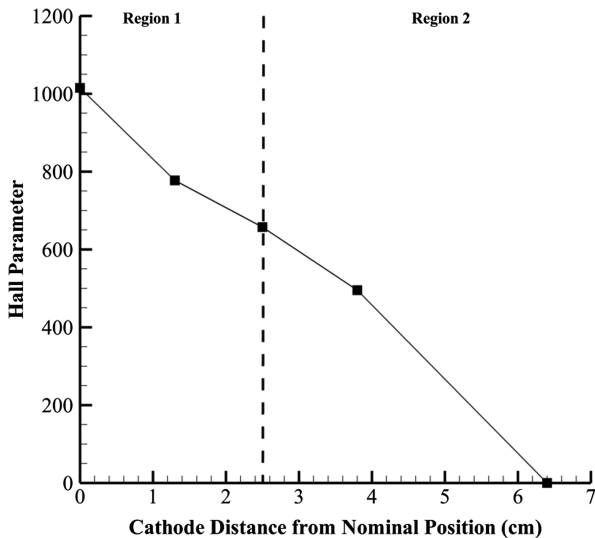


**Fig. 8** Approximate cathode electron Hall parameter as a function of cathode distance from the nominal position.

within region 1. The estimated cathode electron temperature and neutral density are averages based on experimental measurements taken near the exit plane of the SPT-100, which is a HET in the same discharge power class as the T-140 HET; the variation of neutral density with distance from the thruster exit was assumed to follow an inverse-square dependency [6,50]. The results of these calculations are shown in Fig. 8 and reveal that the cathode electrons remain highly magnetized ( $\Omega_e^2 \gg 1$ ) for all cathode locations within this region; thus, the electron motion is restricted to follow the magnetic field lines [6,47].

As shown in Fig. 9, the strong magnetic field forces the electrons to move along magnetic field lines into the thruster channel and towards portions of the thruster body, and therefore, restricts motion into plume or towards the radial plate. The electron current collected by the grounded thruster body is thus maximized and reaches an average value equal to approximately 13% of the discharge current for all plate configurations. This significant current draw drains electrons from the near-field region and leaves only the highest energy electrons able to escape into the plume. The corresponding electron depletion from the near-field plasma pushes the plasma potential higher to maintain a quasi-neutral bulk plasma [51,52]. Once the body is floated, however, this current pathway no longer exists and some of the electrons that were previously collected by the body are able to proceed into the plume. This eases electron transport to the bulk plasma and the plasma potential can equilibrate at a lower value

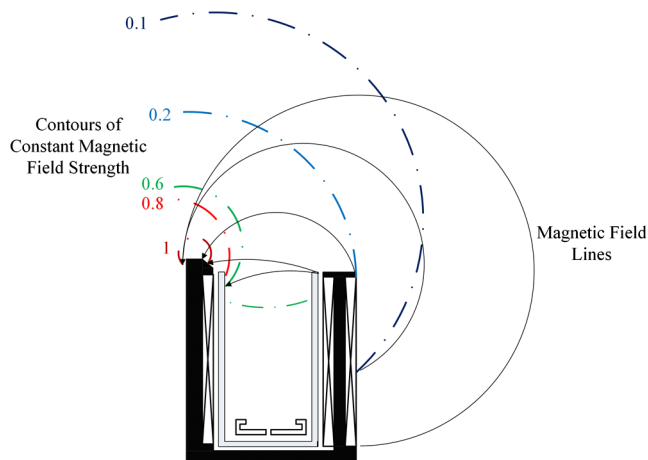


**Fig. 9** Representative magnetic field topology of the T-140 HET; HET centerline is on the left. Dash-dot lines represent iso-field strength contours; solid lines represent magnetic field lines.

for the floating body configurations as compared to the grounded body configurations [51,52]. Please note that the strength of each contour shown in Fig. 9 is given on the left as a fraction of maximum magnetic field for all regions outside of the iron flux guides.

The magnetization of the cathode electrons and the resultant effects on plasma potential in this region also explain the trends observed for the plate and thruster body floating voltages. The increased plasma potential axially downstream of the thruster forces the floating voltage of the axial plate to maximize in order to attract a sufficient number of plume electrons to counter the ion flux caused by the line-of-sight plume impingement, and thus maintain the net-zero current condition [18,47]. Similarly, the increased electron flux toward the thruster body caused by the magnetized electron paths causes the thruster body to float more negative in order to repel a sufficient number of electrons to maintain a net-zero current draw [47].

The magnetization of electrons for cathode positions within this region restricts all but the highest-energy electrons from moving toward the radial plate [6,47]. As the floating voltage is proportional to the electron temperature, the filtering of all but the highest-energy electrons from reaching the radial plate by the HET magnetic field causes the magnitude of the floating voltage on the radial plate to maximize [6]. As the current conducted between the axial plate and radial plate is driven by the difference in floating voltages developed on these two surfaces, the plate-to-plate current maximizes within this region due to aforementioned results of electron magnetization on the plate floating potentials [18].

The increase in plasma potential also drives the electron current collected on the grounded axial and radial plates. Previous work has shown that current collection by the axial and radial plates is similar to current collection by planar Langmuir probes [18,19]. As shown in Fig. 5b, within region 1, grounding the axial plate results in the plate potential being lower than the floating potential. Thus, the plate is effectively in the ion saturation region of the I-V characteristic, and the corresponding electron current collected by the plate is minimized [18,19,44,45]. Similarly, the grounded radial plate is biased above the plate floating voltage, and thus is in the transition region of the I-V characteristic [18,19,44,45]. The result is minimal electron collection by the radial plate due to the small voltage difference between the grounded potential and plate floating potential within region 1. The magnetic field structure, by restricting electron motion, thus forces a significant number of ions to travel to ground through the facility surfaces while forcing electron grounding through the thruster body [18].

As the cathode is moved radially outward from the thruster body, the electrons are forced to follow field lines with increasingly large positive magnetic field gradients. This gradient results in an increase in magnetic mirror force exerted on the electrons, and thus a corresponding increase in electron motion transverse to the magnetic field [48]. The resulting transverse motion decreases the forced travel of electrons to the thruster body, and thus causes the observed decrease with increasing cathode displacement of electron current collected by the grounded thruster body and the floating voltage of the floating thruster body. This transverse motion also permits easier electron transport into the plume and, thus, for the grounded thruster body case, a decrease in the floating voltage of the axial plate. The decreased axial plate floating voltage thus moves the grounded-plate potential closer to the floating potential of the plate, and therefore increases the electron current collected by the plate as a function of cathode displacement within region 1.

## 2. Region 2

As shown in Fig. 4a, for cathode positions within region 2, the current collected by both the grounded axial and radial plates decreases with increasing radial cathode displacement. This trend is also true for the magnitudes of the floating voltage measurements for both the axial and radial plates shown in Figs. 5a and 5b, as well as the current collected by the grounded thruster body and the floating voltage of the floating thruster body shown in Fig. 6. As shown in Fig. 7, within region 2, the plasma potential initially maximizes and

then decreases to a constant-value asymptote with increasing cathode displacement.

These trends are due to the changes in magnetic field strength at the cathode orifice for cathode positions within region 2. Table 1 and Fig. 8 show that, as the radial cathode displacement is increased within region 2, the magnetic field strength (and thus Hall parameter) at the cathode orifice decreases to nearly 0 G. Therefore, as the cathode is moved radially outward within region 2, cathode electrons increasingly lose magnetization and are no longer confined to follow the magnetic field lines shown in Fig. 9. This increasingly permits cathode electrons to move unconstrained into the HET plume by following the spatial potential gradient between the cathode and the plume.

This decrease in restriction of electron motion leads to the observed decrease in the magnitude of the plasma potential and the floating voltages of the thruster body, axial plate, and radial plate. As electrons are freely able to move into the plume, the plasma potential is able to decrease and becomes set by the downstream loss rate of electrons to the facility walls, which should remain nearly invariant due to the nonchanging nature of the downstream chamber surfaces [6,47]. Following the plasma potential, the axial plate must float to a less positive voltage in order to attract the required number of electrons to overcome the ion flux caused by the line-of-sight plume impingement and achieve the required net-zero-current boundary condition [18,47]. Similarly, as electron motion is increasingly unconstrained, the electrons near the radial plate are no longer only the highest-energy ones that are able to escape magnetization. Therefore, the average electron temperature near the radial plate likely decreases and the radial plate must float to a less negative voltage in order to repel the required number of electrons to maintain zero current collection. As the current conducted between the axial plate and radial plate is driven by the difference in floating voltage developed on these two surfaces, the plate-to-plate current decreases within this region as the difference in floating voltage between the axial and radial plates also decreases due to the loss of electron magnetization [18].

As mentioned previously, the current collection by the grounded axial and radial plates is governed by the difference between the plate floating potential and ground. As the axial plate floating voltage decreases toward ground potential with increasing cathode displacement in this region, the axial plate approaches the transition region of the I-V characteristic and the corresponding net collected ion current decreases due to increased electron collection [18,19]. Similarly, as the radial plate floating voltage increases toward ground potential, the net electron current collected by the radial plate also decreases.

The trends observed for the plasma potential within region 2 are also present for the measured thruster body floating voltage shown in Fig. 6. Specifically, both the plasma potential and thruster body floating voltage increase for cathode positions between the boundary of region 1 and 10 cm away from the nominal location then decrease toward a constant-value asymptote for the remaining cathode locations within region 2. The initial increase in plasma potential at the boundary between regions 1 and 2 is likely due to the intersection of the spreading cathode plume with regions of a high magnetic field. This intersection decreases the mobility of the electrons, and thus causes elevated plasma potentials as discussed for region 1. This effect diminishes as the cathode is moved further outward in region 2, as the required spreading angle for the cathode jet to intersect the high magnetic field regions near the thruster increases beyond the cathode plume divergence angle [53–55]. The changes in thruster floating voltage are likely due to the changes in plasma potential. In other words, increases in the plasma potential result in a corresponding increase in the thruster body floating voltage in order to maintain the net-zero-current boundary condition [18,47].

Within this region, fewer electrons are also forced toward the thruster body; thus, the thruster body collects less electron current. As the magnetic field continually drops in this region, the restriction of electron motion also continually drops while the magnetic field gradient between the cathode and thruster body continually increases. This leads to the observed continual decrease in current

collected by the body within region 2, followed by the flattening of this curve once the magnetic field reaches zero at the cathode orifice.

### 3. Region 3

Figure 4a shows that, within region 3, the ion current collected by the grounded axial plate and the electron current collected by the grounded radial plate increase with increasing cathode displacement. As shown in Fig. 5b, this trend is also followed by the magnitude of the floating voltages of both the floating axial and radial plates as well as the current conducted between them. However, the current collected by the grounded thruster body as well as the floating voltage of the floating thruster body, shown in Fig. 6, decrease with increasing cathode displacement within this region.

Unlike in region 1 and region 2, changes in the near-orifice magnetic field cannot account for the observed trends because, as shown in Table 1, the magnetic field strength at the orifice reaches 0 G within region 2 and remains at this value throughout the remainder of region 2 and into region 3. Instead, these trends are explained by geometry. In the near field, the plume of a hollow cathode resembles a jet profile [53–55]. As such, the densest region of plasma lies within a finite half-angle centered on the cathode orifice and the direction of bulk motion of most of the emitted particles is contained within this half-angle. As the cathode is moved closer to the radial plate for positions within region 3, a larger percentage of the cathode plume intersects the radial plate, thus increasing the flux of electrons to the plate.

To confirm this, it is possible to estimate the cathode plume half-angle required for line-of-sight impingement on the radial plate at each radial cathode location within region 3. Neglecting spreading effects, and noting that the cathode orifice was centered on the radial plate, the cathode plume half-angle required for the plume to intersect the radial plate at the boundary between region 2 and region 3 is approximately 75 deg. This required angle is larger than those observed in previous work by Crofton and Boyd, which measured non-negligible ion current for plume solid angles only up to 60 deg [56]. However, these measurements are likely an underestimate of the relevant cathode plume divergence angle for this work due to the higher flow rate of the EPL HCPEE cathode as compared to the one used by Crofton and Boyd [56]. Additional electrons would also likely impinge upon the radial plate due to the neglected effects of spreading and collisional motion. The required cathode plume solid angle to intersect the radial plate decreases to approximately 60 deg for cathode displacements beyond 1 m away from the nominal position. As shown in Fig. 4a, these cathode locations are where the largest increase in radial plate current is observed. Therefore, these calculations suggest that impingement is likely the primary mechanism driving the increased electron current collection by the radial plate within region 3 and that spreading and collisional effects drive impingement for cathode positions between the boundary with region 2 and 1 m away from the nominal position while direct line-of-sight impingement dominates for cathode displacements beyond 1 m.

Impingement effects are the cause of the observed response of the current collected on the grounded axial and radial plates to increasing cathode displacement. The increased electron flux toward the radial plate drives the collected radial plate electron current upward and, correspondingly, causes the floating voltage of the radial plate to decrease in the floating-plate configuration. This line-of-sight impingement effectively limits the electron transport to the plume and forces the plasma potential, and thus the axial plate floating voltage, to increase. This causes the grounded axial plate to be further away from the floating potential on the plate I-V characteristic, and thus the electron current collected on the axial plate to decrease. The distance between the thruster body and the cathode also causes the electron current collected by the grounded thruster body and the magnitude of the floating voltage of the floating thruster body to minimize, as the thruster body is impinged upon by an increasingly small number of electrons.

### 4. Electron Recombination Pathways

The identified regional behavior corresponds with changes in the recombination pathways taken by cathode electrons in the HET

circuit. On-orbit recombination occurs via ion–electron recombination collisions in the HET plume [57]. However, since the ion–electron recombination collision rates in a HET plume are small, the corresponding recombination mean free paths exceed the axial dimension of the ground-test facility [18,19,57]. As such, not all ions and electrons recombine collisionally during ground testing. Instead, those ions and electrons that have not undergone collisional recombination before striking the facility conduct their charge to ground through the facility walls [18,19]. As the facility walls are at a fixed bias, the surface-integrated current collection of ions and electrons across the facility surfaces must balance. Thus, any ion that collides with the wall will recombine with an electron collected elsewhere by the facility.

For this work, the facility pathway was subdivided into two branches: the facility walls and the thruster body. In the grounded thruster body configuration, the thruster body is electrically connected to the test facility, and it acts as part of the facility recombination pathway. However, in order to determine the relative importance of this recombination pathway on the HET circuit, the current collected by the thruster body is shown separately from the current collected by the plates. These pathways are shown graphically in Fig. 10. It is important to note that the other grounded facility surfaces in close proximity to the thruster, including the thrust stand, personnel gratings, and all associated framing, are not included for this work. As such, the thruster body serves as a representative witness electrode for these surfaces in the same way that the axial and radial plates serve as witness electrodes for the axial and radial chamber surfaces, respectively.

The aforementioned results indicate that the primary effect of cathode position is to change the electron current collected by each of these pathways. In region 1, the magnetization of electrons caused a larger number of electrons to travel to through the thruster body to ground, and therefore made the thruster body a significant pathway for electrons to ground. Within region 2, the reduction in magnetic field caused a corresponding decrease in magnetization, and therefore permitted easier electron transport to the thruster plume. However, because the facility dimensions are still shorter than the ion–electron recombination mean free path, recombination increasingly occurred via charged particles impacting the downstream facility surfaces. In region 3, the proximity of the cathode to the radial facility walls increased the electron flux in that direction, and therefore made the radial facility walls a significant electron recombination pathway. Thus, any process dependent upon the path of the electrons through the plasma (including plasma reactance and resistance) may be significantly different between ground operation and operation on orbit, as well as between different cathode placement regions [18–21].

The impact of these changing electron pathways on the plasma density distribution can be seen in Figs. 11a and 11b, which show the ion  $n_i$  and electron  $n_e$  number densities, respectively, measured by the Langmuir probe 1 m downstream of the exit plane of the T-140 HET along the thruster centerline as a function of cathode displacement for each of the plate and thruster body electrical configurations. The average ion and electron number densities for all cathode locations and plate configurations are  $4.49 \times 10^{16} \text{ m}^{-3}$  and  $1.62 \times 10^{16} \text{ m}^{-3}$ , respectively. Within the uncertainty of the measurements, the electron and ion number densities are equal and unchanging for all cathode locations and electrical configurations of the thruster body and plates. As previous results have shown, typical multiply charged ion species fractions of less than 0.01 at discharge voltages of 300 V, the ion population of the T-140 HET can be approximated as singly charged [41]. Within this approximation, the measured equivalence of electron and ion number densities implies that quasi-neutrality is maintained for all cathode locations and plate and thruster body electrical configurations [6,47]. This result is expected, as the Debye length in the vicinity of the Langmuir probe calculated using the measured average ion density of  $4.49 \times 10^{16} \text{ m}^{-3}$  and electron temperature of 4 eV is on the order of  $10 \text{ } \mu\text{m}$ . Since the spatial scale of the plume is much larger than several Debye lengths and HET plume conditions are not conducive to double layer formation, Debye shielding ensures that quasi-neutrality

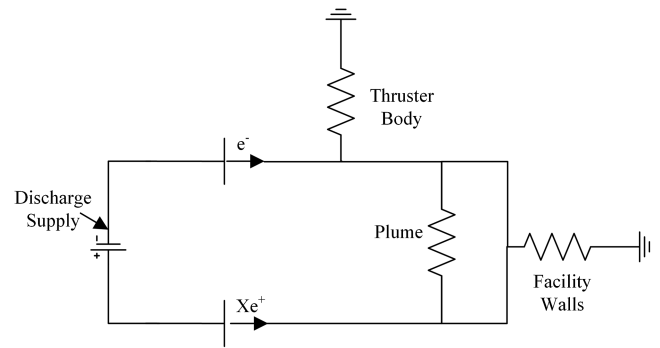


Fig. 10 HET discharge circuit including the recombination pathways available during ground testing.

is maintained throughout the plume despite the observed changes in electron collection characteristics as a function of cathode position by the various facility surfaces [6].

#### D. Effects of Regional Behavior on the HET Circuit

Previous work has identified that the changes to the plasma potential affect the HET circuit via corresponding impacts to the cathode-to-ground voltage [18,19]. Therefore, in order to understand the effect of changing the distribution of electrons between each recombination pathway has on the HET circuit as a whole, the corresponding changes in cathode-to-ground voltage must be analyzed.

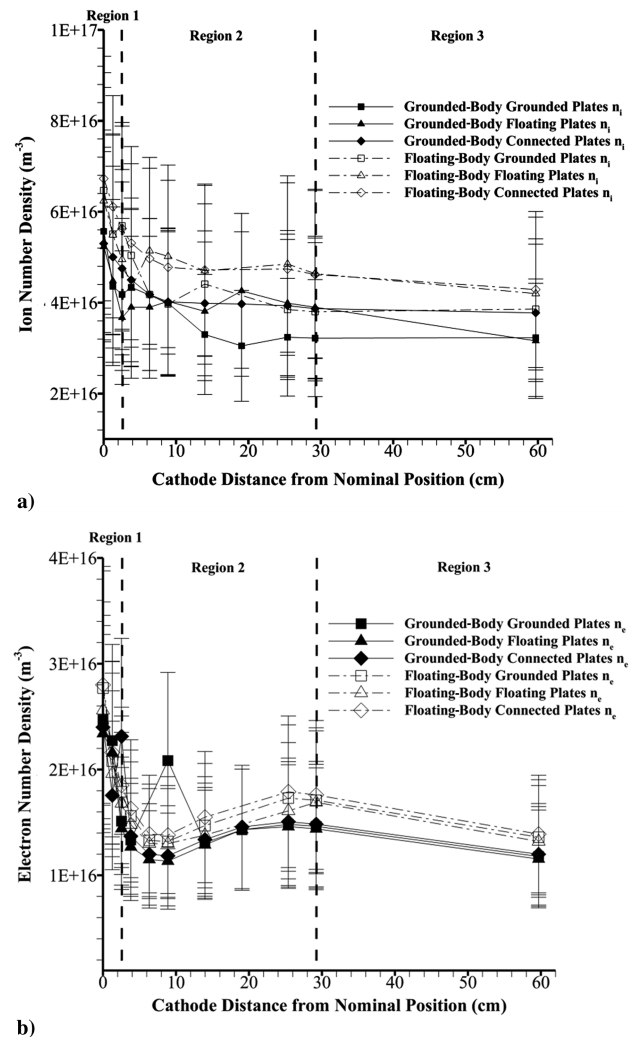


Fig. 11 a) Ion number densities and b) electron number densities as a function of cathode position for all thruster body and plate electrical configurations.

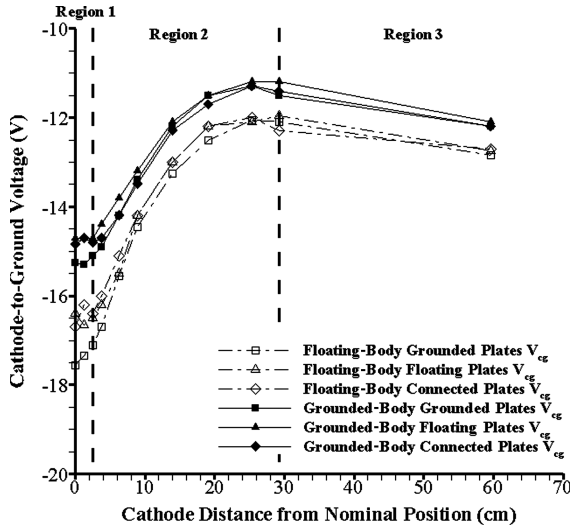


Fig. 12 Cathode-to-ground voltage as a function of cathode distance from nominal position for all thruster body and plate electrical configurations. Experimental error is within the symbol borders.

### 1. Region 1

Figure 12 shows the cathode-to-ground voltage,  $V_{cg}$ , of the T-140 HET measured as a function of radial cathode displacement from the nominal position for each combination of thruster body and plate electrical configurations. Also included in Fig. 12 are the regional demarcations defined in Fig. 4a. In region 1, the cathode-to-ground voltage for the grounded-body grounded-plate configuration changes minimally and stays within 1% of the value recorded at the nominal cathode position. This is consistent for all plate and thruster body electrical configurations. The measurements of cathode-to-ground voltage in Fig. 12 show a dependence on body electrical configuration similar to that of the plasma potential. Specifically, the cathode-to-ground voltages measured in the floating-body configuration are, on average, 9% less than those measured in the grounded thruster body configuration.

The response of the cathode-to-ground voltage is related to that of the plasma potential by the coupling voltage of the cathode. The coupling voltage is a loss term that is defined as the difference between the plasma potential and the cathode-to-ground voltage and indicates the resistance to electron transport between the cathode and HET plume [6,21,58]. The cathode coupling voltage for the grounded thruster body/grounded-plate configuration is shown as a function of cathode displacement in Fig. 13. The cathode coupling voltages for all of the other thruster body and plate configurations are similar and, as such, all trends discussed for this configuration are representative of the results for the other configurations. Within the uncertainty, Fig. 13 shows that the cathode coupling voltage maximizes between regions 1 and 2. The reason for this is that cathode magnetization in this region constrains electron motion, and therefore increases the effective resistance to electron transport. As indicated by Fig. 13, this resistance increases as the cathode is moved outward in this region due to the transverse magnetic mirror force that develops as electrons are forced to cross increasing magnetic field gradients in order to reach the plume.

### 2. Regions 2 and 3

Figure 12 shows that, for orifice locations within region 2, the cathode-to-ground voltages measured for all plate and thruster electrical body configurations follow the trends observed for the plasma potentials shown in Fig. 7. Specifically, the magnitude of the cathode-to-ground voltage decreases with increasing cathode displacement within region 2, and then begins to level off near the transition between region 2 and region 3. The magnitude of this decrease is approximately 24% across region 2. Figure 13 shows that this results in a corresponding decrease in cathode coupling voltage. These decreases are due to the loss of electron magnetization, and

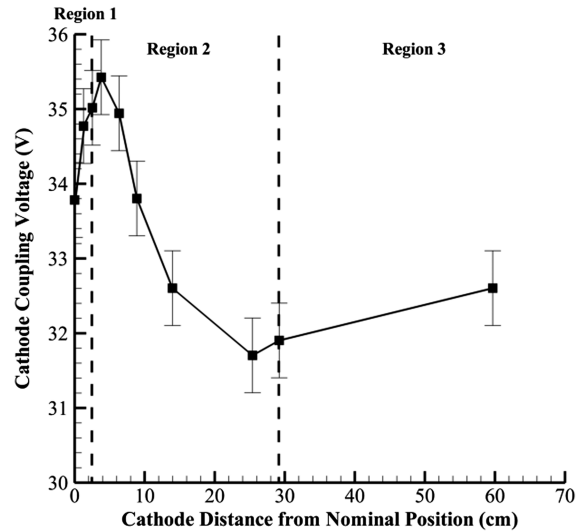


Fig. 13 Cathode coupling voltage as a function of cathode distance from the nominal position for the grounded-body grounded-plate configuration.

therefore the increased ease of cathode electron transport to the plume via electrostatic forces outside of the HET magnetic field. These trends persist into region 3 because, as shown by the radial plate current in Fig. 4a, at the cathode displacement for which the plasma potential and cathode-to-ground voltage were measured, a significant increase in the flux of electrons to the radial plate had not yet occurred.

### E. Effects of Electron Recombination Pathways on Thruster Performance

The net effect of the changing electron recombination pathways on HET performance can be determined from the thrust and RPA measurements. The measured thrust and most probable ion voltages of the T-140 HET as a function of cathode displacement are shown for all plate and thruster body electrical configurations in Figs. 14 and 15, respectively. The T-140 HET produced 178 mN of thrust, and the most probable ion voltage was 251 V. These measurements were invariant (within the experimental uncertainty) for all measured cathode locations within region 1 and variations in plate and thruster body electrical configurations. As shown in Figs. 14 and 15, for orifice locations within region 2, the measured thrust/most probable ion voltages do appear to trend upward as the cathode is moved outward in region 2; however, the shift is within the experimental uncertainty, and it is therefore inconclusive as to whether the HET performance does increase within this region.

These results indicate that, despite the observed changes in electron pathways, the performance and operation of the T-140 HET was largely unaffected. This result is not unexpected as the Debye length in the lower-density less energetic far-field plasma is on the order of  $70 \mu\text{m}$ , which is orders of magnitude less than the spacing between the HET and the plates [18,19,47]. Thus, the bulk plasma interacting with the HET is shielded from the plates, and the HET operates independently of the downstream recombination pathway of beam ions and electrons [18,19,47].

Nevertheless, the measurements taken in this work do match the trends previously observed by Sommerville and King at similar cathode displacements [26]. However, unlike with the work of Sommerville and King, the changes observed for the T-140 HET cannot be attributed to the shape of the magnetic field (i.e., the presence of a separatrix surface) but rather are attributed to the change in electron current collection pathways due to the loss of magnetization in region 2 (i.e., the strength of the magnetic field) [21,33]. It is also interesting to note that the cathode-to-ground voltage trends shown for region 3 in Fig. 12 match results previously acquired for similar cathode locations by Walker and Gallimore [27]. As such, it is possible that the decreases in cathode-to-ground voltage

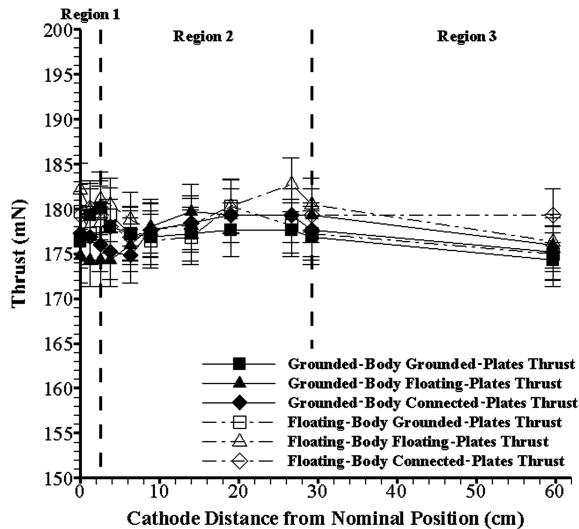


Fig. 14 Thrust measured for the T-140 HET as a function of cathode distance away from the nominal position for all plate and body electrical configurations.

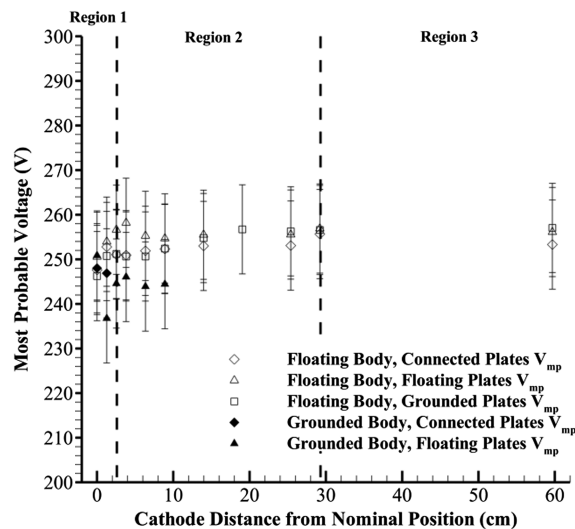


Fig. 15 Most probable ion voltages as a function of cathode position for all thruster body and plate electrical configurations.

observed by Walker and Gallimore were due to an increased resistance to electron transport from the cathode to the HET anode as electrons began to preferentially recombine through the facility wall.

Although much of the presented argument has been focused on recombination, the cathode also sources electrons used for ionization. Furthermore, secondary electrons are created by ionization events within the thruster and may travel toward grounded facility surfaces for collection. A detailed discussion of the electron paths into and out of the channel is outside of the scope of this work, but it may prove a fertile ground for future work into the electrical effects of the test facility on the HET circuit. Nevertheless, the invariance in measured thrust and discharge current suggest that the changing nature of the electron transport as a function of cathode displacement does not dramatically alter the in-channel ionization process.

#### IV. Conclusions

This work experimentally investigated the role of a conductive facility on cathode coupling for a HET. Measurements of the current collected by grounded aluminum witness plates, as well as by the grounded body of the T-140 HET, indicate that the position of the cathode greatly impacts the role played by the conducting vacuum facility in the HET circuit by changing the recombination pathways

taken by the cathode electrons. Specifically, it was shown that these changes exhibit regional behavior with respect to cathode position. For cathode locations near the thruster body, electron magnetization resulted in an increased electron collection by the body, and thus a significant recombination pathway developed through the thruster body to ground. For cathode locations in the midfield radially between the thruster and the facility walls, electrons lost magnetization, were more easily transported into the plume, and were increasingly collected by the downstream chamber surfaces. For cathode locations near the radial facility surfaces, the increased proximity to the radial facility surfaces caused the radial facility surfaces to occupy a significant fraction of the cathode plume half-angle, and thus caused the emergence of an electron pathway through the radial facility surfaces to ground. However, the changing current collection characteristics of the facility surfaces did not appear to cause a loss of plume quasi-neutrality.

Despite the observed changes in electron pathway distributions, measurements of the thruster performance showed no discernible changes as a function of cathode position. Nevertheless, the collection of a significant electron current by the various facility pathways suggests that the presence of the vacuum facility walls and the position of the cathode relative to them significantly alters the path of the electrons, therefore, any processes dependent upon the path of the electrons (e.g., plasma reactivity and resistance) may be different between facility operation and operation in space. These differences may need to be accounted for during ground testing, HET electrical system design, or plasma modeling.

#### Acknowledgments

Jason Frieman and Jonathan Walker are supported by the National Science Foundation Graduate Research Fellowship under grant no. DGE-1148903. The authors would like to thank Sam Langendorf, Natalie Schloeder, and Aaron Schinder for their very helpful assistance in the collection of data and preparation of this manuscript.

#### References

- [1] Brophy, J. R., Friedman, L., and Culik, F., "Asteroid Retrieval Feasibility," *2012 IEEE Aerospace Conference*, IEEE Publ., Piscataway, NJ, 2012, pp. 1–16.
- [2] Semenkina, A., Kim, V., Gorshkov, O., and Jankovsky, R., "Development of Electric Propulsion Standards-Current Status and Further Activity," *Proceedings of the 27th International Electric Propulsion Conference*, Electric Rocket Propulsion Soc., IEPC Paper 2001-070, Fairview Park, OH, 2001.
- [3] Brown, D. L., and Gallimore, A. D., "Evaluation of Plume Divergence and Facility Effects on Far-Field Faraday Probe Current Density Profiles," *31st International Electric Propulsion Conference*, Electric Rocket Propulsion Soc., IEPC Paper 2009-030, Fairview Park, OH, 2009.
- [4] Diamant, K. D., Spektor, R., Beiting, E. J., Young, J. A., and Curtiss, T. J., "The Effects of Background Pressure on Hall Thruster Operation," *48th AIAA/ASME/SAE/ASEE Joint Propulsion Conference and Exhibit*, AIAA Paper 2012-3735, 2012.
- [5] Diamant, K. D., Liang, R., and Corey, R. L., "The Effect of Background Pressure on SPT-100 Hall Thruster Performance," *50th AIAA/ASME/SAE/ASEE Joint Propulsion Conference and Exhibit*, AIAA Paper 2014-3710, 2014. doi:10.2514/6.2014-3710
- [6] Goebel, D. M., and Katz, I., *Fundamentals of Electric Propulsion: Ion and Hall Thrusters*, Wiley, Hoboken, NJ, 2008, pp. 325–341.
- [7] Hofer, R. R., Peterson, P. Y., and Gallimore, A. D., "Characterizing Vacuum Facility Backpressure Effects on the Performance of a Hall Thruster," *27th International Electric Propulsion Conference*, Electric Rocket Propulsion Soc., IEPC Paper 2001-045, Fairview Park, OH, 2001.
- [8] Hofer, R. R., and Anderson, J. R., "Finite Pressure Effects in Magnetically Shielded Hall Thrusters," *50th AIAA/ASME/SAE/ASEE Joint Propulsion Conference and Exhibit*, AIAA Paper 2014-3709, 2014. doi:10.2514/6.2014-3709
- [9] Huang, W., Kamhawi, H., Lobbia, R. B., and Brown, D. L., "Effect of Background Pressure on the Plasma Oscillation Characteristics of the HiVHAc Hall Thruster," *50th AIAA/ASME/SAE/ASEE Joint Propulsion*

- Conference and Exhibit*, AIAA Paper 2014-3708, 2014.  
doi:10.2514/6.2014-3708
- [10] Kamhawi, H., Huang, W., Haag, T., and Spektor, R., "Investigation of the Effects of Facility Background Pressure on the Performance and Voltage-Current Characteristics of the High Voltage Hall Accelerator," *50th AIAA/ASME/SAE/ASEE Joint Propulsion Conference and Exhibit*, AIAA Paper 2014-3707, 2014.  
doi:10.2514/6.2014-3707
- [11] Nakles, M. R., and Hargus, W. A., "Background Pressure Effects on Ion Velocity Distribution Within a Medium-Power Hall Thruster," *Journal of Propulsion and Power*, Vol. 27, No. 4, 2011, pp. 737-743.  
doi:10.2514/1.48027
- [12] Randolph, T., Kim, V., Kaufman, H. R., Kozubsky, K., Zhurin, V. V., and Day, M., "Facility Effects on Stationary Plasma Thruster Testing," *23rd International Electric Propulsion Conference*, Electric Rocket Propulsion Soc., IEPC Paper 1993-093, Fairview Park, OH, 1993.
- [13] Reid, B. M., "The Influence of Neutral Flow Rate in the Operation of Hall Thrusters," Ph.D. Dissertation, Aerospace Engineering Dept., Univ. of Michigan, Ann Arbor, MI, 2009, pp. 306-319.
- [14] Walker, M. L. R., "Effects of Facility Backpressure on the Performance and Plume of a Hall Thruster," Ph.D. Dissertation, Aerospace Engineering Dept., Univ. of Michigan, Ann Arbor, MI, 2005, pp. 126-135.
- [15] Walker, M. L. R., Hofer, R. R., and Gallimore, A. D., "The Effects of Nude Faraday Probe Design and Vacuum Facility Backpressure on the Measured Ion Current Density Profile of Hall Thruster Plumes," *38th AIAA/ASME/SAE/ASEE Joint Propulsion Conference and Exhibit*, AIAA Paper 2002-4253, 2002.
- [16] Walker, M. L. R., Victor, A. L., Hofer, R. R., and Gallimore, A. D., "Effect of Backpressure on Ion Current Density Measurements in Hall Thruster Plumes," *Journal of Propulsion and Power*, Vol. 21, No. 3, 2005, pp. 408-415.  
doi:10.2514/1.7713
- [17] Azziz, Y., Martinez-Sanchez, M., and Szabo, J. J., "Determination of In-Orbit Plume Characteristics from Laboratory Measurements," *42nd AIAA/ASME/SAE/ASEE Joint Propulsion Conference and Exhibit*, AIAA Paper 2006-4484, 2006.  
doi:10.2514/6.2006-4484
- [18] Frieman, J. D., King, S. T., Walker, M. L. R., Khayms, V., and King, D., "Role of a Conducting Vacuum Chamber in the Hall Effect Thruster Electrical Circuit," *Journal of Propulsion and Power*, Vol. 30, No. 6, 2014, pp. 1471-1479.  
doi:10.2514/1.B35308
- [19] Frieman, J. D., King, S. T., Walker, M. L. R., Khayms, V., and King, D., "Preliminary Assessment of the Role of a Conducting Vacuum Chamber in the Hall Effect Thruster Electrical Circuit," *50th AIAA/ASME/SAE/ASEE Joint Propulsion Conference and Exhibit*, AIAA Paper 2014-3712, 2014.  
doi:10.2514/6.2014-3712
- [20] Sommerville, J. D., and King, L. B., "Hall-Effect Thruster-Cathode Coupling, Part II: Ion Beam and Near-Field Plume," *Journal of Propulsion and Power*, Vol. 27, No. 4, 2011, pp. 754-767.  
doi:10.2514/1.50124
- [21] Sommerville, J. D., and King, L. B., "Hall-Effect Thruster-Cathode Coupling, Part I: Efficiency Improvements from an Extended Outer Pole," *Journal of Propulsion and Power*, Vol. 27, No. 4, 2011, pp. 744-753.  
doi:10.2514/1.50123
- [22] Tilley, D. L., de Grys, K. H., and Myers, R. M., "Hall Thruster-Cathode Coupling," *35th AIAA/ASME/SAE/ASEE Joint Propulsion Conference and Exhibit*, AIAA Paper 1999-2865, 1999.
- [23] Albarede, L., Lago, V., Lasgorceix, P., Dudeck, M., Bugrova, A. I., and Malik, K., "Interaction of a Hollow Cathode Stream with a Hall Thruster," *28th International Electric Propulsion Conference*, Electric Rocket Propulsion Soc., IEPC Paper 2003-333, Fairview Park, OH, 2003.
- [24] Hofer, R., Johnson, L., Goebel, D. M., and Fitzgerald, D., "Effects of an Internally-Mounted Cathode on Hall Thruster Plume Properties," *42nd AIAA/ASME/SAE/ASEE Joint Propulsion Conference and Exhibit*, AIAA Paper 2006-4482, 2006.  
doi:10.2514/6.2006-4482
- [25] Jameson, K. K., Goebel, D. M., Hofer, R., and Watkins, R. M., "Cathode Coupling in Hall Thrusters," *30th International Electric Propulsion Conference*, Electric Rocket Propulsion Soc., IEPC Paper 2007-278, Fairview Park, OH, 2007.
- [26] Sommerville, J. D., and King, L. B., "Effect of Cathode Position on Hall-Effect Thruster Performance and Cathode Coupling Voltage," *43rd AIAA/ASME/SAE/ASEE Joint Propulsion Conference and Exhibit*, AIAA Paper 2007-5174, 2007.
- [27] Walker, M. L. R., and Gallimore, A. D., "Hall Thruster Cluster Operation with a Shared Cathode," *Journal of Propulsion and Power*, Vol. 23, No. 3, 2007, pp. 528-536.  
doi:10.2514/1.23688
- [28] Kieckhafer, A. W., and Walker, M. L. R., "Recirculating Liquid Nitrogen System for Operation of Cryogenic Pumps," *32nd International Electric Propulsion Conference*, Electric Rocket Propulsion Soc., IEPC Paper 2011-217, Fairview Park, OH, 2011.
- [29] Walker, M. L. R., and Gallimore, A. D., "Neutral Density Map of Hall Thruster Plume Expansion in a Vacuum Chamber," *Review of Scientific Instruments*, Vol. 76, No. 5, 2005, Paper 053509.  
doi:10.1063/1.1915011
- [30] Dushman, S., and Lafferty, J. M., *Scientific Foundations of Vacuum Technique*, Wiley, New York, 1962, pp. 349-359.
- [31] McLean, C. H., McVey, J. B., and Schappell, D. T., "Testing of a U.S.-Built HET System for Orbit Transfer Applications," *35th AIAA/ASME/SAE/ASEE Joint Propulsion Conference and Exhibit*, AIAA Paper 1999-2574, 1999.  
doi:10.2514/6.1999-2574
- [32] Snyder, J. S., Baldwin, J., Frieman, J. D., Walker, M. L. R., Hicks, N. S., Polzin, K. A., and Singleton, J. T., "Flow Control and Measurement in Electric Propulsion Systems: Towards an AIAA Reference Standard," *33rd International Electric Propulsion Conference*, Electric Rocket Propulsion Soc., IEPC Paper 2013-425, Fairview Park, OH, 2013.
- [33] Walker, J. A., Frieman, J. D., Walker, M. L. R., and Khayms, V., "Hall Effect Thruster Electrical Interaction with a Conductive Vacuum Chamber," *50th AIAA/ASME/SAE/ASEE Joint Propulsion Conference and Exhibit*, AIAA Paper 2014-3711, 2014.  
doi:10.2514/6.2014-3711
- [34] Martinez, R. A., Dao, H., and Walker, M. L. R., "Power Deposition into the Discharge Channel of a Hall Effect Thruster," *Journal of Propulsion and Power*, Vol. 30, No. 1, 2014, pp. 209-220.  
doi:10.2514/1.B34897
- [35] Kurzyina, J., Mazouffre, S., Lazurenko, A., Albarede, L., Bonhomme, G., Makowski, K., Dudeck, M., and Peradzynski, Z., "Spectral Analysis of Hall-Effect Thruster Plasma Oscillations Based on the Empirical Mode Decomposition," *Physics of Plasmas*, Vol. 12, No. 12, 2005, Paper 123506.  
doi:10.1063/1.2145020
- [36] Litvak, A., Raitses, Y., and Fisch, N., "Experimental Studies of High Frequency Oscillations in Hall Thrusters," *38th AIAA/ASME/SAE/ASEE Joint Propulsion Conference and Exhibit*, AIAA Paper 2002-3825, 2002.  
doi:10.2514/6.2002-3825
- [37] Xu, K. G., and Walker, M. L. R., "High-Power, Null-Type, Inverted Pendulum Thrust Stand," *Review of Scientific Instruments*, Vol. 80, No. 5, 2009, Paper 055103.  
doi:10.1063/1.3125626
- [38] Absalamov, S., Andreev, V., Colbert, T., Day, M., Egorov, V., Gnizdor, R., Kaufman, H., Kim, V., Koriakin, A., Kozubsky, K., Kudravzev, S., Lebedev, U., Popov, G., and Zhurin, V., "Measurement of Plasma Parameters in the Stationary Plasma Thruster (SPT-100) Plume and its Effect on Spacecraft Components," *28th AIAA/ASME/SAE/ASEE Joint Propulsion Conference and Exhibit*, AIAA Paper 1992-3156, 1992.
- [39] King, L. B., "Transport-Property and Mass Spectral Measurements in the Plasma Exhaust Plume of a Hall-Effect Space Propulsion System," Ph.D. Dissertation, Aerospace Engineering Dept., Univ. of Michigan, Ann Arbor, MI, 1998, pp. 42-48.
- [40] Xu, K. G., "Ion Collimation and In-Channel Potential Shaping using In-Channel Electrodes for Hall Effect Thrusters," Ph.D. Dissertation, Aerospace Engineering Dept., Georgia Inst. of Technology, Atlanta, 2012, pp. 48-53.
- [41] Hofer, R., "Development and Characterization of High-Efficiency, High-Specific Impulse Xenon Hall Thrusters," Ph.D. Dissertation, Aerospace Engineering Dept., Univ. of Michigan, Ann Arbor, MI, 2004, pp. 267-274, 281-284.
- [42] Sheehan, J. P., and Hershkowitz, N., "Emissive Probes," *Plasma Sources Science and Technology*, Vol. 20, No. 6, 2011, Paper 063001.  
doi:10.1088/0963-0252/20/6/063001
- [43] Jakubowski, A. K., "Effect of Angle of Incidence on the Response of Cylindrical Electrostatic Probes at Supersonic Speeds," *AIAA Journal*, Vol. 10, No. 8, 1972, pp. 988-995.  
doi:10.2514/3.50282
- [44] Demidov, V. I., Ratynskaia, S. V., and Rypdal, K., "Electric Probes for Plasmas: The Link Between Theory and Instrument," *Review of*

- Scientific Instruments*, Vol. 73, No. 10, 2002, pp. 3409–3439.  
doi:10.1063/1.1505099
- [45] Hutchinson, I. H., *Principles of Plasma Diagnostics*, Cambridge Univ. Press, Cambridge, England, U.K., 2002, pp. 55–72.
- [46] Haas, J., Gulczinski, F. S., III, Gallimore, A., Spanjers, G. G., and Spores, R. A., “Performance Characteristics of a 5 kW Laboratory Hall Thruster,” *34th AIAA/ASME/SAE/ASEE Joint Propulsion Conference and Exhibit*, AIAA Paper 1998-3503, 1998.
- [47] Piel, A., *Plasma Physics an Introduction to Laboratory, Space, and Fusion Plasmas*, Springer-Verlag, Berlin, 2010, pp. 1411–1426.
- [48] Fossum, E., “Electron Transport in E x B Devices,” Ph.D. Dissertation, Dept. of Mechanical Engineering, Michigan Technological Univ., Houghton, MI, 2009, pp. 13–52.
- [49] Katz, I., Anderson, J. R., Polk, J. E., and Brophy, J. R., “One-Dimensional Hollow Cathode Model,” *Journal of Propulsion and Power*, Vol. 19, No. 4, 2003, pp. 595–600.  
doi:10.2514/2.6146
- [50] Boyd, I. D., “A Review of Hall Thruster Plume Modeling,” *38th Aerospace Sciences Meeting and Exhibit*, AIAA Paper 2000-0466, 2000.  
doi:10.2514/6.2000-466
- [51] Logue, M. D., Shin, H., Zhu, W., Xu, L., Donnelly, V. M., Economou, D. J., and Kushner, M. J., “Ion Energy Distributions in Inductively Coupled Plasmas Having a Biased Boundary Electrode,” *Plasma Sources Science and Technology*, Vol. 21, No. 6, 2012, Paper 065009.  
doi:10.1088/0963-0252/21/6/065009
- [52] Shin, H., Zhu, W., Xu, L., Donnelly, V. M., and Economou, D. J., “Control of Ion Energy Distributions Using a Pulsed Plasma with Synchronous Bias on a Boundary Electrode,” *Plasma Sources Science and Technology*, Vol. 20, No. 5, 2011, Paper 055001.  
doi:10.1088/0963-0252/20/5/055001
- [53] Boyd, I. D., and Dressler, R. A., “Far Field Modeling of the Plasma Plume of a Hall Thruster,” *Journal of Applied Physics*, Vol. 92, No. 4, 2002, pp. 1764–1774.
- [54] Jameson, K., Goebel, D., Mikellides, I., and Watkins, R., “Local Neutral Density and Plasma Parameter Measurements in a Hollow Cathode Plume,” *42nd AIAA/ASME/SAE/ASEE Joint Propulsion Conference and Exhibit*, AIAA Paper 2006-4490, 2006.  
doi:10.2514/6.2006-4490
- [55] Mikellides, I., Katz, I., Jameson, K., and Goebel, D., “Driving Processes in the Orifice and Near-Plume Regions of a Hollow Cathode,” *42nd AIAA/ASME/SAE/ASEE Joint Propulsion Conference and Exhibit*, AIAA Paper 2006-5151, 2006.
- [56] Crofton, M., and Boyd, I., “Plume Measurement and Modeling Results for a Xenon Hollow Cathode,” *38th AIAA/ASME/SAE/ASEE Joint Propulsion Conference and Exhibit*, AIAA Paper 2002-4103, 2002.
- [57] Jahn, R. G., *Physics of Electric Propulsion*, McGraw-Hill, New York, 1968, pp. 45–68.
- [58] McDonald, M. S., and Gallimore, A. D., “Cathode Position and Orientation Effects on Cathode Coupling in a 6-kW Hall Thruster,” *31st International Electric Propulsion Conference*, Electric Rocket Propulsion Soc., IEPC Paper 2009-113, Fairview Park, OH, 2009.

J. Blandino  
Associate Editor